NASA Contractor Report 179619

Optical Strain Measurement System Development—Phase I

(NASA-CR-179619) OPTICAL STRAIN MEASUREMENT SYSTEM DEVELOPMENT, PHASE 1 Final Report (Sverdrup Technology) 39 p Avail: NTIS HC A03/MF A01 CSCL 14B

N87-22960

Unclas G3/35 0076843

Christian T. Lant and Walid Qaqish
Sverdrup Technology, Inc.
Lewis Research Center
Cleveland, Ohio

May 1987

Prepared for the
Lewis Research Center
Under Contract NAS3-24105

National Aeronautics and
Space Administration

OPTICAL STRAIN MEASUREMENT SYSTEM DEVELOPMENT - PHASE I

Christian T. Lant and Walid Qaqish
Sverdrup Technology, Inc.
Lewis Research Center
Cleveland, Ohio 44135

1.0. SUMMARY

This contract has covered the first of a multiphase effort in developing an optical strain gauge capable of mapping in two dimensions the strain on the surface of a hot specimen. Testing of the durability of propulsion system components prompted the need for such instrumentation. The objective of this first phase has been to provide a noncontact, one-dimensional, differential strain gauge for experimental purposes.

The optical strain measurement system that has been developed in this phase-one effort is based on the technique introduced by Ichirou Yamaguchi (ref. 1). The displacement of speckle patterns generated by a test specimen subject to stress is directly proportional to surface strain. The use of two symmetrically incident laser beams allows automatic cancellation of speckle translation terms due to rigid body motion. The resolution of the optical system is 16 microstrain in the present configuration, and strain has successfully been measured up to a specimen temperature of 450 °C, in an open air environment. The upper temperature limit is determined by dynamic refractive gradients in the air between the specimen and the sensor. The strain measurement error is ±18 microstrain ±0.3 percent of the strain reading.

Measurement procedures of the system are controlled by an operator through the terminal of a microcomputer. The data input to the computer consists of unshifted (reference) speckle patterns and shifted speckle patterns from a linear photodiode array, positional information of the test specimen from an area photodiode array, temperature readings, stress values, and strain measured from conventional resistance strain gauges mounted on the specimen. The area photodiode array monitors the location of the laser spots on the specimen, which is the gauge position. The gauge position can be changed by using motorized mirror mounts interfaced to the computer to relocate the laser spots to a new location on the specimen. The area array is also used to store a "snapshot" of the test specimen and the laser spot position so that there is a graphic record of the location of each strain data point.

E-3550

2.0 INTRODUCTION

2.1 Task Identification

Investigations of physical phenomena affecting the durability of space shuttle main engine (SSME) components require the development of measurement systems operable in hostile environments. The need for such instrumentation defined this program to develop a noncontact optical strain measurement system for these investigations.

This final report covers the task entitled the Optical Strain Measurement System Development. Sverdrup Technology, Inc. is developing this optical strain measurement system in the NASA Lewis Research Center's Instrument Research Laboratory. This task is the first of a multiphase effort to establish an in-house R&D capability of optical strain measurement, which will be used to map in two dimensions the strain field on the surface of a hot specimen. This first phase is to provide a noncontact, one-dimensional optical strain gauge for experimental purposes.

2.2 Background

The design of the optical strain gauge is based on the speckle shift method of Ichirou Yamaguchi (ref. 1) at the Institute of Physical and Chemical Research, Japan. Laser speckle is a phase effect caused by the diffuse reflection of spatially coherent light off of a rough surface. Interference of the light reflected off a specimen results in a light and dark intensity distribution at the sensor. Yamaguchi's noncontact method of measuring differential (i.e., not absolute) surface strain makes use of speckle displacement detected by cross-correlating electrical signals from a linear photodiode array. The speckle displacement due to stress on the test specimen is directly proportional to the associated strain. Use of this method eliminates problems usually caused by subjecting measurement devices to hostile environments such as extreme temperatures, and high electromagnetic fields; the sensor need not be in the same environment as the specimen. In addition, Yamaguchi's method has the advantages over other optical strain measurement techniques (refs. 2 and 3) of not only being noncontacting, but needing no surface preparation, automatically correcting for strain error due to rigid body motion, and giving quasi-real time results (the value of strain is calculated within seconds of taking the data). Although Stetson's speckle photogrammetry technique records in detail the encoded strain distribution over a surface, extensive post-processing is required to extract the strain data. Sharpe's interferometric technique requires the surface to be prepared with reflective indentations, limiting its mapping flexibility.

2.3 Objectives

Although Yamaguchi's technique was chosen to adapt to the Optical Strain Measurement System, very little specific data was available as to this strain measurement technique's range of applications. Questions pertaining to its maximum effective open air temperature limit, the typical range of error introduced by out-of-plane displacement, and its adaptability toward automation in a test facility environment needed to be answered. This experiment as a whole was designed to answer these questions and obtain first-hand knowledge of the strong and weak points of Yamaguchi's speckle strain technique, with satisfaction of the SSME durability needs being the long-range goal.

2.4 General Procedures

Testing of the system consisted primarily of measuring stress-strain relations of flat specimens of Inconel 600 at different temperatures. At various temperature set points the specimens were stepped through a range of tensile loads, while the strain was measured optically and also by conventional

resistance strain gauges. The resulting stress-strain data were compared to published and measured values of the moduli of elasticity to determine the accuracy of the instrument. Thermal strain was also measured by the optical system.

3.0 THEORY

3.1 Speckle Shift Relations

The utilization of laser speckle to determine differential strain is achieved by applying the Fresnel-Kirchhoff diffraction integral describing the propagation of light in free space. This integral is an approximation of the more rigorous Helmholtz-Kirchhoff theorem stemming from the wave equation for light. The Fresnel-Kirchhoff equation then is used to derive the relationship between surface deformation of a specimen subject to loading and speckle displacement in the diffraction field (refs. 1 and 4). The speckle displacement contains terms of translation, rotation, and strain, from which the strain term must be extracted. This extraction relies on the use of two symmetrically placed laser beams reflected sequentially onto a linear photodiode array located parallel to the specimen surface. After the reference (before-strain) and shifted (after-strain) speckle patterns from each beam are correlated, the difference in speckle shift between them is taken leaving only the component due to surface strain (ref. 1).

Referring to the general coordinate system shown in figure 1, a laser beam is incident on the diffuse surface of a test specimen at an angle to the surface. The observation plane is the X,Y plane, and the object plane is the lowercase x,y plane. The center of the incident laser spot is at the origin O of the x,y plane. When the object is stressed and deformed, the object point $r(x,y)$ is displaced by $a(x,y)$. The unit vector in the directions of the center of curvature S of the incident wavefront and the observation point Q are denoted by $\ell s(\ell s_X, \ell s_Y, \ell s_Z)$ and $\ell(\ell_X, \ell_Y, \ell_Z)$, respectively, directed away from the origin O. The radius of curvature of the wavefront is denoted Ls. The speckle displacement $\bar{A}$ is broken down into components in the X,Y plane, given by

$$A_X = -a_x\left[\frac{Lo}{Ls}\left(\ell s_x^2 - 1\right) + \ell_x^2 - 1\right] - a_y\left[\frac{Lo}{Ls}\,\ell s_x \ell s_y + \ell_x \ell_y\right] - a_z\left[\frac{Lo}{Ls}\,\ell s_x \ell s_z + \ell_x \ell_z\right]$$
$$- Lo\left[\varepsilon_{xx}\left(\ell s_x + \ell_x\right) + \varepsilon_{xy}\left(\ell s_y + \ell_y\right) - \Omega_y\left(\ell s_z + \ell_z\right) + \Omega_z\left(\ell s_y + \ell_y\right)\right] \qquad (1a)$$

$$A_Y = -a_x\left[\frac{Lo}{Ls}\,\ell s_y \ell s_x + \ell_y \ell_x\right] - a_y\left[\frac{Lo}{Ls}\left(\ell s_y^2 - 1\right) + \ell_y^2 - 1\right] - a_z\left[\frac{Lo}{Ls}\,\ell s_y \ell s_z + \ell_y \ell_z\right]$$
$$- Lo\left[\varepsilon_{yy}\left(\ell s_y + \ell_y\right) + \varepsilon_{xy}\left(\ell s_x + \ell_x\right) - \Omega_x\left(\ell s_z + \ell_z\right) - \Omega_z\left(\ell s_x + \ell_x\right)\right] \qquad (1b)$$

where $\bar{a}$, $\bar{\Omega}$, and $[\tilde{\varepsilon}]$ are the translation vector, the rotation vector, and the strain tensor, respectively, defined as follows, assuming plane strain:

$$(a_x, a_y, a_z) = [a_x(0,0),\ a_y(0,0),\ a_z(0,0)] \qquad (2)$$

$$(\Omega_x, \Omega_y, \Omega_z) = \left\{ \left(\frac{\partial a_z}{\partial y}\right)_0, -\left(\frac{\partial a_z}{\partial x}\right)_0, \frac{1}{2}\left[\left(\frac{\partial a_y}{\partial x}\right)_0 - \left(\frac{\partial a_x}{\partial y}\right)_0\right] \right\} \tag{3}$$

$$\epsilon_{xx} = \left(\frac{\partial a_x}{\partial x}\right)_0; \quad \epsilon_{yy} = \left(\frac{\partial a_y}{\partial y}\right)_0 \tag{4a,b}$$

$$\epsilon_{xy} = \epsilon_{yx} = \frac{1}{2}\left[\left(\frac{\partial a_y}{\partial x}\right)_0 + \left(\frac{\partial a_x}{\partial y}\right)_0\right] \tag{4c,d}$$

The theory interpreting the speckle displacement in the observation plane is based on the assumption that the illuminated region of the specimen is homogeneous. It is this region that acts as a random diffraction grating, thus for speckle shift to accurately represent strain requires that the change in the surface roughness spacing be uniform. This proved to be the case in the experimentation within the elastic limit of the test specimen, as observed in the stability of the speckle patterns and the agreement of the results with known quantities.

The configuration shown in figure 2 has two symmetrically incident beams, and simplifies the equations for speckle displacement through the following orientations: the axis of the linear photodiode array is in the plane of incidence, namely the x,z plane, and parallel to the specimen surface at the laser spot location. The position vectors now become $\vec{\ell}s = (\sin\theta_s, 0, \cos\theta_s)$ and $\vec{\ell} = (0,0,1)$. In addition, the incident radius of curvature Ls is much greater than the sensor distance Lo, and Lo is much greater than the spot size w of the incident beam. For each beam, equations (1) now reduce to

$$A_X = a_x - Lo[\epsilon_{xx} \sin\theta_s - \Omega_y(\cos\theta_s + 1)] \tag{5a}$$

$$A_Y = a_y - Lo[\epsilon_{xy} \sin\theta_s - \Omega_x(\cos\theta_s + 1) - \Omega_z \sin\theta_s] \tag{5b}$$

As long as the displacement A_Y is much smaller than the sum of the sensor height and the "typical" speckle size on the sensor (Goodman gives the typical speckle size to be $1.22\,\lambda\,Lo/w$, which also corresponds to the upper limit of the power spectral density of the speckle intensity distribution, i.e., the minimum speckle size (ref. 5)), A_X can be determined by cross-correlating the sensor signals before and after surface deformation. The rotation component Ω_y in A_X can be cancelled out by taking the difference between speckle displacements from the two beams at θ_s and $-\theta_s$. From equation (5a)

$$\Delta A_X = A_X(\theta_s) - A_X(-\theta_s) = -2Lo\epsilon_{xx} \sin\theta \quad \left(\theta = |\theta_s|\right) \tag{6}$$

or finally,

$$\epsilon_{xx} = \frac{-\Delta A_X}{2Lo \sin\theta} \tag{7}$$

The strain in the x direction can now be solved for by

(1) Knowing the geometry of the beam/sensor arrangement

(2) Substituting in the differential speckle displacement ΔA_X obtained from the cross-correlation operations

3.2 Cross-Correlation

The displacement of the speckle patterns due to the strain on the specimen surface must be obtained from a cross-correlation function. The system first acquires four speckle patterns--two reference patterns ($\pm\theta_S$) obtained before applying a load to the specimen, and two patterns ($\pm\theta_S$) shifted due to strain. The mean values of each of the speckle patterns are calculated and subtracted from each sample point before the correlation is performed. The correlation algorithm then, in effect, overlays the shifted speckle pattern onto the reference pattern and varies the relative positions until a maximum in the correlation function indicates the proper amount of shift. This variation-from-the-mean technique of removing a dc offset from the data before the correlation is performed increases the visibility of the peak position of the correlation function. Cross-correlation is given by the following integral:

$$R(\Delta X) = \frac{1}{X}\int_0^X f(X) \cdot g(X + \Delta X)\, dX \qquad (8)$$

where $f(X)$ is the variation from the mean of the reference speckle pattern, $g(X + \Delta X)$ is the variation from the mean of the shifted speckle pattern, and ΔX is the amount of shift. This integral is computed repeatedly for increasing values of ΔX; the value of ΔX for which R is a maximum is the amount of shift A_X between the speckle patterns.

The correlation routine is performed for the reference and the shifted speckle patterns from the left incident beam, and again for the reference and the shifted patterns from the right incident beam. A 750 diode cross-section of each speckle pattern is used in order to minimize the execution time of the measurement. The difference between the values of A_X from the left and right correlations (ΔA_X) is then used in the strain equation (5) to calculate the surface strain.

A typical pair of speckle patterns (reference and shifted) is shown in figure 3, and their cross-correlation function is shown in figure 4. The shift between the speckle patterns was induced by a 13.8 MPa (2 ksi) load. The shift A_X was calculated to the seven diodes (105 μm), corresponding to 65 microstrain on the specimen after rigid body shift was cancelled out. The correlation curve was not normalized, due to the increased execution time involved.

4.0 MEASUREMENT SYSTEM DESIGN AND SETUP

4.1 System Design

The system is designed to run predominantly under computer control, with the operator selecting procedures from menus on the CRT. A schematic of the

optical setup is depicted in figure 5. The laser and beam steering equipment are mounted on a hard-coupled optical table (this noninterferometric technique does not require vibration isolation). Two variable beamsplitters are used to create three beam paths, each beam switched by an acousto-optic modulator. A line scan camera records the speckle patterns generated by the left and right beams, and an area array camera allows the test section and gauge position to be monitored remotely. The cameras, modulators, and the motorized mirror mounts are remotely controlled. The testing machine and induction heater are mounted on a hydraulic lift table to provide positioning flexibility relative to the optics. An expanded beam provides illumination for the area array camera.

The test specimens are made from Inconel 600 stock, since this is an engine component alloy used for high temperature applications. Another criterion for material selection was that the material would react in a documented and predictable manner throughout the range of experimentation of the measurement system.

The control and data paths are shown in figure 6. The system controller initiates procedures through three main components, these being the data acquisition/control unit (DAQ), and two pulse generators. The data acquisition/control unit outputs control signals to the custom circuitry used for exposing and reading the linear and area array cameras; these circuits synchronize the pulse generators with the array cameras, triggering the pulse generators to output TTL exposure pulses to the acousto-optic modulator RF generators. The triggered outputs of the pulse generators switching on and off the beam-deflecting modulators act as high speed programmable shutters. The DAQ is also used to read the voltages from thermocouples, resistance strain gauges on the specimen, and a load cell. Higher temperatures are also measured by the infrared pyrometer which, in addition, provides PID control of the induction heater through a current control line. This allows precise control of the specimen temperature at the gauge position.

After exposing the linear array the speckle data is read into a waveform recorder in asynchronous mode, digitized to 10 bits, and then transferred via Direct Memory Access (DMA) to a buffer in the system controller. When a pattern each from the left beam and the right beam are stored the correlation is performed against the reference patterns stored at a different load setting, and the calculated strain value is written to a character data array. Strain values are computed over a range of loads, the collection of which comprises a "data run" or "run." The run is then stored on a hard disc ("mass storage unit"), in a file.

From these data runs one can determine the stress-strain characteristics of the material (in particular, the modulus of elasticity), and the accuracy of the data. Comparisons are made graphically between a set of optical gauge data and a set of gauge readings from a standard resistance strain gauge. Plots of the data may be generated on the CRT and transferred to the thermal printer, or a color hard copy may be plotted on the six-pen plotter.

4.2 Equipment Components and Operation

The equipment needed to construct this experimental setup includes optical components, testing equipment and specimens, and a computer system.

The optical equipment consists of:

- 4 W Argon-ion laser
- Acousto-optic modulators
- Motorized mirror mounts
- 2048 element linear photodiode array camera
- 128 by 128 element area photodiode array camera
- Optical table
- Infrared pyrometer
- Assorted optics

The testing equipment includes:

- Horizontal stress fatigue testing machine
- 2.5 kW induction heater generator
- Hydraulic lift table
- Test specimens

The computer system used is comprised of a Hewlett-Packard 236CU controller, with the following peripherals:

- 65.7 Mbyte disc/tape drive
- Data acquisition/control unit (DAQ)
- Extender for the DAQ
- Bus expander
- Waveform recorder
- Programmable pulse/function generators
- Thermal printer
- Plotter

The custom electronics included:

- Linear and area camera exposure and control circuitry
- Driver/receiver interface circuitry

For a listing of equipment model numbers, refer to appendix A. Details of the custom camera control circuitry can be found in appendix B. A brief description of the equipment components and their operation is outlined below.

4.2.1 Optical equipment. - The optical equipment consists of all components dealing with the propagation and detection of the laser light. The components are described in the following sections. Figure 7 is a view of the optical system.

Laser: The light source for the experiment is an Argon ion continuous-wave laser, with a 2 W output at the 514.5 nm wavelength. An Argon laser was chosen for its high power output in order that short exposure times can be used for the photodiode arrays, even when a highly absorbing specimen is being used; this increases the signal to noise ratio, allowing for a more confident correlation peak.

The maximum power output of the 514.5 nm line varies between 1.5 to 2.5 W. The light control is usually set for 2.0 W to provide a stable output beam.

The beam is directed into three legs using high power beamsplitters and beamsteerers. Two of the legs are used to generate the speckle patterns from which the strain values are retrieved, and the third beam is expanded to illuminate the test section for viewing on the monitor. The power split is 40 percent for each of the speckle, or "linear" beams, and 20 percent for the expanded "area" beam.

The gauge length of this speckle shift technique is determined by the spot diameter of the linear beams on the specimen. This spot diameter is a function of the optical resonator and the distance from the beam waist. The setup used in this experiment gives a spot size w, or gauge length, of 5 mm.

Acousto-optic modulators: The acousto-optic modulators (AOM's) are Bragg cells used to deflect the laser beams onto the surface of the specimen. There are three modulators--one for each of the two beams used to produce the speckle patterns, and a third to control the exposure of the test section by the illumination beam.

Each modulator has its own controller, which provides a 40 MHz signal generating acoustic waves in the modulator crystal. The 40 MHz signals are switched by 50 Ω TTL pulses sent to the controllers. These TTL pulses are generated by pulse/function generators, whose outputs are gated to each AOM controller sequentially. The gates are enabled by control inputs sent by the data acquisition unit, as directed by the computer.

The zeroth order beam from each Bragg cell is terminated by a beam stop in between exposures, and the first order maximum during deflection is the exposure beam.

Motorized mirror mounts: While the dual beam system is effective for separating strain from rigid body motion, it is essential that the laser spots remain located at their initial positions on the specimen throughout the measurement. The motorized mounts are for positioning the two speckle-producing laser beams to the same point on the specimen, and for moving the beams to new strain measurement regions. These motorized mounts provide independent rotational control of the mirrors about two orthogonal axes, so each beam can be deflected horizontally and vertically. Each axis has a separate controller that is operated digitally from the data acquisition/control unit. The signals are controlled remotely by the operator from the computer keyboard, which directs an actuator card in the data acquisition unit to output the proper combination of control signals. Differential line drivers send these signals across the laboratory, where they are converted to TTL levels for direct input to the mirror controller edge card connectors.

Photodiode arrays: There are two photodiode array cameras in the system--a 2048 element linear array (or line scan) camera and a 128 by 128 element matrix (or area) array camera. The linear array is the one used to read the speckle patterns generated by the specimen, and the area array provides a picture of the specimen and the measurement point for the operator at the computer terminal. This picture is used in conjunction with the motorized mirror mounts to position the laser spots on the specimen.

The linear array has a 15 μm pitch between diode centers, and a diode height of 16 μm. The center-to-center spacing of the area matrix array elements is 60 μm. The line scan camera uses a clear glass window in front of the

array elements for protection, and an interference filter to attenuate all wavelengths but the 514.5 nm laser line. The area array camera is used with a telephoto lens to image and magnify the test section.

Both arrays are housed in electronic cameras, each with a controller that is interfaced to the data acquisition system by a custom exposure control circuit. The line scan camera is controlled under external start mode and both cameras are self-scanning using their internal clocks, each running at about 1 MHz. The integration time for the diodes depends on the exposure control circuitry, but is automatically limited to a maximum of 40 ms. The analog diode voltage levels are transmitted over coaxial lines to the waveform recorder in synchronous mode, whereupon the waveform recorder digitizes the signals and transmits them via a GPIO data bus to a buffer in the computer.

Infrared pryometer: An IR pyrometer provides a local temperature reading of the specimen, and is in keeping with the noncontacting philosophy of the system. The pyrometer uses blackbody statistics relating radiation emission levels to temperature, and is sensitive around the 2 μm wavelength. Its temperature range is from 350 to 800 °C. A three mode controller is incorporated into the unit, and controls the power output of the induction heater used to heat the specimen. A BCD output of the pyrometer's temperature reading is transmitted to the data acquisition unit's digital input card, and entered into the computer for storage in the data array.

Assorted optics: Other optical components include variable polarizing beamsplitters, interference filters (optimized at 514.5 nm), beamsteerers and mirrors, translation and rotational stages, an optical table, and a beam expander/collimator. Optical coatings and thermally stable substrates suitable for high power laser applications were used where necessary.

Figure 8 shows the camera controllers, the IR pyrometer controller, acousto-optic modulator RF generators, and a motorized mirror mount controller. Also seen in figure 8 is a manual beam switching panel connected to the modulator RF generators.

4.2.2 Test equipment and specimens. - Figure 9 is a view of the test system, comprised of a testing machine, RF induction heater, and specimens, all mounted on a hydraulic lift table.

Horizontal fatigue testing machine: The direct stress fatigue machine was used for static loading only. A handcrank was provided for preloading the specimen, and a load arm connected to an eccentric crank was used to vary the load statically during testing. A horizontal configuration was used in order to simplify the optical setup.

The test specimen was held by clevis grips attached to water-cooled extensions, in order to protect the load cell from overheating. The cooling extensions were fabricated from Inconel X stock, onto which copper tubing was brazed.

RF induction heater: The induction heater (fig. 10) provided up to 2.5 kW of radio frequency energy to the specimen. Induction heating was chosen for three reasons. First, the setup provided for ready optical access to the specimen during heating; second, an open air configuration could be used; and third, it was a noncontacting heat source.

The power was transmitted to the specimen over a water cooled coaxial line fabricated in-house. The induction coil was made of 0.63 cm (0.25 in.) copper tubing wound into six 2.54 cm (1.00 in.) diameter coils.

Hydraulic lift table: The lift table provided a stable, moveable base onto which the testing machine and the induction heater could be mounted.

Test specimens: The three test specimens used throughout this experimentation were fabricated from Inconel 600 stock. A pin loaded flat specimen configuration was used, and the reduced section was 63.5 mm (2.50 in.) long, 12.7 mm (0.500 in.) wide, and 1.6 mm (0.062 in.) thick.

Each specimen was instrumented for a different purpose. The first specimen (specimen 1, shown in fig. 11) was fully instrumented with resistance strain gauges and thermocouples, and was intended for low temperature testing. Three resistance strain gauges were bonded to the back of the specimen, with the sensitive axes along the load (x) axis. These gauges were spaced 12.5 mm apart, with a gauge length of 1.6 mm. In addition, a pair of orthogonal gauges were bonded to each side of the specimen to measure bending. Two type "K" thermocouples were mounted 12.5 mm apart, one on either side of the center of the test section, measuring the surface temperature.

Specimen 2, shown in figure 12, had only thermocouples mounted on it, for use in high temperature testing. Nine thermocouples in all were mounted on the specimen: four thermocouples were arranged in a diamond shape on the front of the specimen (to allow optical access to the center); the remaining five were arranged similarly on the back, with the fifth thermocouple in the center of the specimen. The thermocouples were spaced 12.5 mm apart, measured along the specimen axes.

The remaining specimen, specimen 3, had no instrumentation attached to it, relying solely on the optical instruments to measure temperature and strain.

4.2.3 Computer equipment. - The computer equipment consists of all equipment addressable by the HPIB interface (fig. 13). Details of each component are given in the following paragraphs.

65.7 Mbyte disc/tape drive: This hard disc/tape drive was used to store and back-up all software and data for the system. The disc was formatted for the Pascal multidirectory file system, with a large main directory accessible to BASIC.

Data acquisition/control unit and extender: The data acquisition unit was used to read thermocouples, resistance strain gauges, and the load cell, as well as a BCD temperature input from the IR pyrometer. It also served as a digital control for the motorized mirror mounts, and the camera exposure control circuitry. The extender provided additional slots for I/O card assembles.

Bus expander: This unit served as a backplane slot expander to the system controller. It provided additional slots for parallel ports and RAM cards.

Waveform recorder: The waveform recorder was used as a high speed A/D converter and buffer for the linear and area camera video signals. The digitized video data was transferred by a GPIO bus, using direct memory access, to a buffer in the system controller for correlation.

Programmable pulse/function generator: There were two pulse generators, one to provide triggered pulses to the modulators switching the speckle generating laser beams, and one for sending pulses for the expanded area beam. The widths of the pulses output by these pulse generators were set by a subprogram in the main program, in response to an operator provided interrupt. This allows the operator to change the exposure time of the cameras according to the power output of the laser, and the reflectance of the specimen surface.

Plotter: This six pen plotter was used to graph color plots of the stress-strain data generated by the data runs.

Thermal printer: The thermal printer provided a hard copy of the run data in tabular form. It was also used as a graphics dump device, to provide a quick hard copy of the graphical data displayed on the CRT.

4.3 Custom Electronics

Custom circuit boards were designed to interface the linear array and area array cameras/controllers to the waveform recorder, as well as to synchronize the speckle exposure pulses with the camera scan rates. Control lines set by the system controller via the DAQ allowed external control of these circuits. The controls determined which of the two cameras was on-line with the waveform recorder, and which of the three exposure beams was being pulsed.

The exposure pulses to the beam modulators were provided by two programmable pulse generators, triggered by the Custom Camera Control circuits at the appropriate points in the array scanning periods. One pulse generator was used for both the left and right unexpanded speckle exposure laser beams (used by both the linear and area arrays cameras), and the second pulse generator provided the exposure pulse for the low power expanded (area) beam, used to illuminate the test section for the area array camera. The pulse widths were programmed into the pulse generators, as needed, by the system controller via HPIB interfaces.

4.4 Software

The computer ran on the Hewlett-Packard BASIC operating system, which was convenient for the input/output operations that were needed to tie the system together. This operating system was a structured version of BASIC containing powerful programming features such as error recovery, a wide variety of event-initiated interrupts, extensive graphics features, and flexible I/O capabilities. These features, combined with a program prerun that set up pointer tables and memory maps to increase execution speed, made HPBASIC an excellent choice for controlling the system.

The main program was written in the HPBASIC language, and performed all functions needed to collect and store speckle patterns and other data generated by the testing. Once this data was stored in memory, a Hewlett-Packard utility called compiled subroutine (CSUB) was invoked to perform the correlation of the speckle patterns. This CSUB utility allowed a precompiled Pascal language subroutine to be called by the BASIC main program, in order to perform the correlation at a speed much greater than that permitted by the interpreted language of BASIC. This configuration let the speed advantage of compiled code be used

for the lengthy calculations required by the correlation function, while the strong features of HPBASIC were still available to the remainder of the data-taking algorithms.

4.4.1 Main program. - The procedures for the experiment were controlled through the execution of branches in the main program. The operator decided what functions were to be invoked to procure the needed data, and then chose keyboard activated interrupts to initiate the required branch. Each branch was a subroutine that called the subprograms needed to complete the procedure.

The program prompts (branches) included a selection of individual steps in the procedure, in addition to predefined sequences of the more commonly used steps. Each prompt directed execution of the program to a subroutine that called the appropriate subprograms. These subprograms were executed in sequence until the end of the subroutine was reached, whereupon the program returned to the menu block to idle until the next prompt was selected.

Flexibility was the goal behind this program design. The result was that the operator could either run through an automated strain measurement procedure, or select specific operations to perform in whatever sequence was needed at the time.

4.4.2 Subroutines. - Subroutines provided the framework of the experiment. They were the link between the operator and the functions the computer was to perform. As the operator chose each subroutine from a menu on the CRT, the subroutine invoked a series of instrument-controlling and data-taking subprograms. What follows are some examples of subroutines used in the experiment:

- Update a reference speckle pattern
- Adjust the laser spot position
- Measure a strain value
- Store data on magnetic media
- Record surface temperature and reference strain gauge readings
- Automatically take strain measurements at manually adjusted stress settings
- Plot stress-strain relations

Some of these routines performed simple, explicit tasks while others, such as the one for taking automatic strain measurements, performed all the functions and prompting needed to obtain a stress-strain curve for the specimen.

5.0 EXPERIMENTAL DESIGN AND PROCEDURE

5.1 Test Procedure

The goals defined in section 2.3 provided most of the framework needed to design a sequence of tests, or runs, illustrating the properties of this strain measurement system. The overall sequence of tests were: (1) measurement of stress-strain relations from unaxial mechanical loading at room temperature; (2) isothermal strain measurements at high temperatures; and (3) thermally induced strain measurement, with temperatures ranging from 350 to 800 °C, with negligible mechanical loading.

These tests were performed using two distinct techniques. The first technique, called here the "absolute shift" technique, compared the shifted speckle patterns from each strain measurement point to the same pair of reference patterns, taken at the beginning of the run. This technique was used to determine the stability of the speckle patterns over a range of strain, and the degree of correlation between the reference and shifted patterns throughout this same range.

The second technique, dubbed the "relative shift," or "incremental shift" technique, updated the reference patterns for each strain value with the shifted patterns from the previous strain value measured. The strain recorded at any stress point was then the sum total of the previous strain increments since the beginning of the run.

Every load or thermal cycle was preceded with the storage of two unstrained, reference speckle patterns--one from the left laser beam and one from the right beam, and the "zero load" voltages of the load cell and resistance strain gauges. It was this set of reference patterns that the strained (shifted) speckle patterns were correlated against to determine the spatial shift. One of the objectives of this experiment was to determine how much shift a pattern could undergo before correlation with the reference pattern was undetectable. In general, the sequence of steps leading to a data point on the specimen was the following:

At the beginning of the run (a) preload the specimen to seat load axis couplings; (b) align the specimen with the load axis to minimize rigid body motion (RBM) induced speckle movement; (c) align laser spots on the specimen; (d) store the reference voltages of the load cell and the resistance strain gauges; and (e) store the reference speckle pattern for each beam.

Then, for each successive strain point in the run (f) update the reference patterns with the shifted patterns from the previous point (incremental shift method only); (g) apply a load to the specimen; (h) read the shifted speckle pattern for each beam; (i) correlate the reference and shifted patterns for each beam, where the peaks of the correlation functions give the total shift for each beam; (j) take the difference between the displacements of the two patterns to cancel rigid body motion; (k) calculate the strain from the remaining shift; and (l) store the stress, strain, and temperature values.

Careful alignment of the specimen in the testing machine was critical, in order to minimize rigid body motion of the test specimen. In particular, three components of excessive RBM were intolerable. The z component of specimen translation, a_z, caused an error in the strain value directly proportional to the differential magnitude of a_z. The maximum allowable value of a_z was 0.1 mm. The other two components of RBM that needed to be minimized were the rotational term about the x axis, Ω_x, and the translation component in the y direction, a_y. Both of these terms led to a speckle shift in the sensor plane in the Y direction, A_Y (eq. (5b)). No observable error resulted from A_Y, but as stated in the theory section of this report, a value of A_Y greater than the sum of the sensor height and the minimum speckle size resulted in decorrelation between the speckle patterns, causing a value of strain random in magnitude and sign to be returned from the correlation routine.

Therefore, steps (a) and (b) above were needed to minimize these three components. Step (a) prevented gross movements of the specimen by removing slack from the load components. Step (b) reduced bending of the specimen, as well as other components of load not along the x axis.

A number of runs were performed for each of the three types of tests conducted. Specific steps in each procedure are listed in the sections to follow; each run of a particular procedure may have differed slightly in the preload value of the stress increments used, but the values given are typical.

5.1.1 Mechanically induced strain. - The experiment began with the measurement of strain induced by mechanical loading of the test specimen, using the absolute shift technique. Specimen 1 was placed in the horizontal stress fatigue testing machine, with resistance strain gauges and thermocouples attached to the reverse side of the specimen to provide reference data.

In a typical run, the specimen was placed under a 34 to 69 MPa (5.0 to 10.0 ksi) preload, which was treated as the zero load point when reading load cell and resistance gauge reference voltages. Unless specified otherwise, all stress values given in this report will assume a preload offset. The run began after adjusting the load axis of the tensile machine to minimize rigid body motion.

The reference speckle patterns were recorded, then the "shifted" patterns were taken without changing the load. This verified the zero strain point of the run and was also used to observe temporal stability of the speckle patterns, especially during high temperature runs. The stress was increased to 6.9 MPa (1.0 ksi), and a new pair of shifted speckle patterns was recorded and correlated with the reference pattern pair. The sequence of incrementing the stress on the specimen by 6.9 to 21 MPa (1.0 to 3.0 ksi), storing a pair of shifted speckle patterns, and calculating the strain was repeated until decorrelation occurred between the original reference patterns and the final pair of shifted patterns. The data array for the run was then stored on the hard disc, and the data were analyzed.

The incremental shift method was tested using a procedure very similar to that of the absolute shift method described above. For the incremental shift technique, the pair of shifted patterns generated at the most recent value of stress was correlated with the pair associated with the previous load state, and the resulting strain added to the running total.

5.1.2 Isothermal strain relations at higher temperatures. - The next step of the experiment was to produce accurate isothermal stress-strain curves at the highest temperature possible, using specimen 2. An RF induction heater under external proportional-integral-derivative (PID) control was used to heat the specimen. Before the testing began, the specimen was cycled through the temperature range to stabilize surface oxidation. The temperature of the specimen was held at 600 °C for about 5 min, and then returned to room temperature. The temperature was then fixed at 400 °C for 30 min prior to the run, to insure a steady-state temperature distribution. The temperature continued to be held constant while the mechanical load was varied and the strain values measured, as per the procedure in section 5.1.1. This procedure was repeated for a temperature set point of 450 °C, with good results. At temperatures higher than 450 °C, using the absolute shift technique, decorrelation became too severe to accurately determine strain.

5.1.3 Thermally induced strain. - The final objective of the experiment was to determine the reliability of this optical strain measurement system to measure the thermal expansion of a test specimen. As before, an induction heater was used to heat the specimen. The procedure was to allow free expansion of the specimen as the temperature set-point was increased--the specimen was not in a preload state.

The operating range of the pyrometer PID control output for the RF heater was 350 to 800 °C. For this reason, thermal strain tests were conducted from 350 to 450 °C, where dynamic refractive gradients were observed to cause excessive pattern degradation. From 350 °C the temperature setpoint was increased in 1 to 10° increments and allowed to stabilize before storing a shifted pattern pair and calculating the thermal strain. The incremental shift technique was used due to excessive A_Y movement of the patterns, caused by flexing and shifting of the specimen and load components as the temperature increased.

6.0 RESULTS AND RECOMMENDATIONS

After some minor adjustments were made to the optical paths and the testing machine, a number of data runs were performed with the system, the results of which are detailed in the text to follow. The overall results of the experimentation lead to a favorable rating of the test system as a whole, with the exception of the load transmission components.

Some plots of typical data runs are shown in figures 14 to 18. These figures show data for isothermal runs at room temperature and 450 °C, as well as a run measuring thermal strain. All optical data shown here, except for a technique comparison run in figure 15, were collected using the incremental shift technique.

6.1 Results

Tests conducted during this program verified the stability of speckle patterns generated by an oxidized specimen subject to maximum strains over 0.1 percent. The stability of the surface structure of the specimen was not observed to be affected by high temperature once oxidation occurred. The tests were conducted in an open air atmosphere.

Figure 14 shows the optical gauge data plotted alongside the data from a resistance strain gauge taken at the same time. The curves can be seen to enter the nonlinear region of strain, and their slopes agree to within 6 percent. An offset of 6.9 to 14 MPa (1.0 to 2.0 ksi) occurs at the beginning of the run, where no strain is measured optically. This offset (initially large slope) is typical of the optical measurements at the start of the load cycle, and is believed to be caused by movement of the specimen at small angle deflections of the eccentric crank connected to the load arm of the testing machine. This initial movement is either inherent to the testing machine, or is caused by the skew angle of the clevis grips, or both.

The plots in figure 15 demonstrate the agreement between the methods of "absolute" and "incremental" shift. The two plots represent separate runs taken in succession, under the same set of parameters. The absolute shift run

was conducted first, during which decorrelation occurred at 64 MPa. The load was then relaxed to the initial preload state, and the incremental shift run was conducted using the same load increments as for the absolute shift run. The same initial reference patterns were used for the incremental shift run, so the "zero" load points are the same.

The second data point on the absolute shift curve indicates an apparent strain term, due to specimen translation in the z direction, that does not occur on the incremental shift curve. The effect of this offset remains for the rest of the run, as is observed from the constant offset between the plots. The remainder of the data points follow precisely the same shift (or strain) increments in a parallel progression, indicating that the sum of the correlation resolution error and the error due to translation a_z (after the initial offset in the absolute shift curve) was the same for both methods.

Another important result shown by the runs in figure 15 is the difference in sensitivity to decorrelation between the absolute and incremental shift methods. The run using the absolute shift technique terminated at 63 MPa (9.2 ksi) due to decorrelation from speckle shifts in the Y direction, whereas the run summing incremental strains was continued up to 177 MPa (25.6 ksi). Although runs using the absolute shift method have been successfully conducted up to 0.1 percent strain, the specimen typically moves about enough to cause decorrelation at loads occurring well below this differential range.

Note that before the specimen was strained, the correlation of the reference patterns repeatedly returned a shift of a single diode at the zero load point (indicating a strain of 16 microstrain) for every set of patterns recorded at zero load. The conclusion was drawn that the resolution of the AD/C (10 bits) allowed the correlation peak for this particular pattern to be spread over two values of shift. In the event of equal peak values, the correlation peak-picking routine retains the first peak value encountered, which in this case corresponds to the -1 diode shift index instead of the expected shift index value of zero.

In figures 16(a) and (b), hysteresis due to plastic strain is observed in both the optical and resistance gauge data as the load is backed down to the initial preset value. Both sets of data were generated on the same run. Figure 16(a) shows the plots of the optical gauge data, and figure 16(b) shows the corresponding resistance gauge data. Agreement between the two gauges is very good, with the final offset strain values of the optical and resistance gauges within 2 microstrain of each other. This is well within the resolution of both gauges. Linear fits of the data show differences of 8 percent on the load-up cycle and 3 percent on the load-down cycle.

The optical data curve is discontinuous at the beginning of the load-down cycle, due to the out-of-plane displacement term a_z. This type of break in the curve is often observed as the load is relaxed and the specimen returns to its neutral, unloaded position along the z axis. In figure 16(a), the a_z offset on the load-down cycle is nearly equal to the sum of the a_z offsets in the opposite direction during the load-up cycle. The remaining a_z displacement is spread smoothly along the curve as a function of load. When the plots from each gauge are superposed and offset to align the load-down curves, the slope signatures are the same.

Figure 17 shows stress-strain data at high temperature, using specimen 2. The temperature setpoint was 450 °C, and the incremental shift method was used. The straight line drawn on the plot is the modulus of elasticity E(T = 450 °C) given by an Inconel 600 data sheet. The slope calculated from the optical gauge data is 10 percent higher than the handbook value. The optical data show discontinuities below 67 MPa (10 ksi) due to specimen shifting in the z direction (a_z), but smooths out for a constant slope up to 200 MPa (29 ksi). At high loads, the term a_z has been observed to increase proportionally with load, which accounts for the slightly larger slope of the optical data.

A test run measuring thermal strain is shown in figure 18. The Ircon pyrometer controller was initially set at 350 °C, and then increased by 1° increments as each strain value was measured. The temperature increments were increased to 5° or more as correlation confidence grew, and the data array was filled. A second array was started to finish the temperature ramp, causing a delay of 5 min; a discontinuity appears between the plots of these two sets of data, but the second array continues with the same slope. The delay between the two data arrays was due to a software limitation, and will be eliminated in future testing.

As with the isothermal runs, poor correlation occurred at temperatures above 450 °C, and the run was terminated. A linear fit of the data gives the measured coefficient of expansion to be 14.3 microstrain per degree Celsius. This is within 3 percent of the handbook value. Some random error (±14.8 microstrain) occurred due to the uncertainty in the temperature measurements.

A least-squares regression over the linear portion of the strain data taken for each run provides a good measure of the accuracy of the data. The calculated modulus of elasticity (E) or coefficient of thermal expansion shows error trends in the system (e.g., the error due to a_z increasing with load). The linear-correlation coefficient indicates the degree of confidence in E, or how well strain is shown to be a function of stress. The plots shown here have linear-correlation coefficients ranging from 0.998 to 1.000.

6.2 Error Analysis

The error introduced by the assumptions and approximations in the theory are typically small. Sources of the most significant errors are analyzed below:

(1) The most obvious error in the system is that introduced by the speckle shift detection system, or, that parameter determining the smallest detectable shift. This limit is determined by the diode spacing of the linear array, as long as the detector system can distinguish between adjacent diode signal levels. The full angle width (or the distance between the intensity minima) of the smallest speckle is 165 μm for this optical setup, and the photodiode detector spacing is 15 μm. This gives a diode-to-speckle ratio of about 11, leading to the conclusion that the limiting factor is the diode pitch. The resolution of the system then is a function of the sensor distance Lo, and the diode spacing. The relation is

$$\text{resolution} = 0.707\ [\text{diode spacing}/Lo]$$

For a pitch of 15 μm/diode and a sensor distance of 0.656 m, the resolution is 16 microstrain.

(2) A system requirement is that $Ls >> Lo$ in order to assume a planar treatment of the wavefront. If the ratio $Lo/Ls << 1$ then most of the speckle displacement terms in equation (1a) will drop out of the equation; the remainder of the terms will be canceled due to the sign change of the symmetrically incident beams, leaving only the amount of shift due to strain along the sensor axis. When this inequality is not met, then the differential speckle shift is

$$\Delta A_X = -2Lo\epsilon_{xx} \sin\theta + a_x \cos^2\theta \left[\left(\frac{Lo}{Ls}\right)_R - \left(\frac{Lo}{Ls}\right)_L\right] - a_z \sin\theta \cos\theta \left[\left(\frac{Lo}{Ls}\right)_R + \left(\frac{Lo}{Ls}\right)_L\right]$$

where the subscripts L and R refer to the left and right beam paths, respectively (i.e., the beams at $\pm\theta$).

The worst case is if the ratio for the left incident beam is not equal to the ratio for the right beam. In this worst case situation the surface strain would not be separable from the other terms in equation (1a), and errors would result.

If however, the ratios are made equal for the left and right beams by careful adjustment of the optical path lengths, then the value of strain will be retrievable, provided out-of-plane displacement a_z of the specimen is minimal; that is,

for $[Lo/Ls]_L = [Lo/Ls]_R$

$$\epsilon_{xx} = \frac{-\Delta A_X}{2Lo \sin\theta} - \left[\frac{a_z \cos\theta}{Ls}\right]$$

For the case of the present equal beam path system, the ratio $Lo/Ls = 0.125$ results in the error term equaling $0.13\ a_z$ strain.

A combination of an inherent looseness of the testing machine, poor machining of the specimen grips, and the resulting alignment limitations of the load transmission components has in fact led to excessive out-of-plane movement in a number of runs. This error can be minimized by decreasing the ratio of Lo/Ls, or limiting the a_z term at the source.

(3) If the out-of-plane error in item 2 is eliminated, the remaining error in strain is given by the following total differential equation:

$$\partial\epsilon_{xx} = \frac{-\partial\ \Delta A_X}{2Lo \sin\theta} + \frac{\partial Lo}{Lo}\epsilon_{xx} - \frac{\partial\theta}{\tan\theta}\epsilon_{xx}$$

where

$$\partial\ \Delta A_X = \pm 17\ \mu m$$

$$\partial Lo = \pm 1 \text{ mm}$$

$$\partial \theta = \pm 1.6 \text{ mrad}$$

Therefore,

$$\partial \varepsilon_{xx} = \pm 18 \ \mu\varepsilon \ \pm 0.3 \text{ percent of the strain reading}$$

(4) The inequality $A_Y << [1.22 \ \lambda \ Lo/w + \text{sensor height}]$ is a requirement for correlation of the speckle patterns. It introduces error only if a random correlation peak overshadows the actual peak diminished by decorrelation, or if the peak is flat over a number of diode shifts. The magnitude of A_Y is dependent on the vertical component of strain and translational and rotational components of the specimen. The combined displacement in the image plane must be much less than 98 μm, which independently requires an angular rotation of the specimen of much less than 0.15 mrad, and a vertical translation of much less than 98 μm in the object plane. This requirement is one of the most difficult to meet, since fatigue testing machines are not designed with optical sensitivity in mind, and is in fact often the limiting factor in the range of differential strain measurable from a given reference point (i.e., "absolute shift").

Because of this Y component of speckle shift, the incremental shift technique is a more reliable method to use for most large range strain measurements. No error "walk off" larger than the resolution of the system has been observed when summing incremental strains. In fact, data taken with the incremental technique has a better linear fit than data measured with absolute shifts. This seems to be due to a smearing (flattening) of the peak position of the cross correlation function when A_Y reaches the 98 μm limit.

6.3 Conclusions

The experimentation conducted during this project has resulted in a number of useful insights regarding the implementation of Yamaguchi's theory.

Overall, this measurement system works very well for measuring strain at low to mid-range temperatures (up to 450 °C). Increasing the temperature range depends on how well air density perturbations in the vicinity of the specimen can be controlled. These perturbations cause time-varying speckle intensity fluctuations which lead to a relative shift between the left and right correlation functions. There exist a number of possible configurations that may be used to diminish this problem, the use of which will be left for further developmental stages of this system.

The most practical result of the testing, though, is that the effectiveness of Yamaguchi's speckle shift technique as a strain gauge is limited by the extent of the system's immunity to rigid body motion of the test specimen. Thus, the limiting factors in implementing the test system are terms of rigid body motion. An increase in the radius of curvature of the laser beam wavefront, as well as careful alignment of the specimen in the load train, can eliminate the systematic error observed in these tests and ensure the reliability of the data with minimum equipment specifications.

During much of the testing, an alignment problem usually led to components of rigid body motion in excess of the magnitudes tolerable by the present system parameters. The a_z term of rigid body motion caused by the load components was larger than anticipated, and it contributed an error term to many of the stress-strain measurements taken during testing of the system.

The major contribution to a_z was caused by poor machining of the clevis grips purchased to hold and load the test specimen. The grips screwed into cooling extensions which doubled as couplers between the loading studs and the clevis grips; the problem was that the axis of the threads tapped into each grip was not parallel to the load axis of the specimen. Among the four clevis grips ordered, the angle between threads and the load axis ranged from 3.5 to 8.2 mrad.

Once the problem was discovered the grips could neither be replaced nor omitted from the loading train, but the pair of grips finally used in the testing was chosen such that the angle between the grips was minimized; the alignment of the testing machine was then adjusted so as to minimize a_z when a load was applied. Bending moments at the test section were minimized through careful adjustments to the load axis alignment, and contributed only small strains to the overall measurements. Any remaining bending differential was typically overshadowed by RBM error.

The off-axis load component caused a positive rotation of the specimen about the y axis and a negative translation in the z direction. The rotational term of rigid body motion successfully canceled in the strain equations. However, the translational term a_z did not always completely cancel, due to the finite ratio of Lo/Ls. The error term introduced by this translation caused some offset of each strain value measured, where the magnitude of the offset was usually a function of load. Therefore, the overall error in the results is observed as a scale factor to the modulus of elasticity taken from a linear regression of the strain data for each run. The translation, however, was not always linear with load and could not be predicted as a rule. At times it is observed on the plots that the greatest error occurs at the beginning of the load cycle, and then becomes negligible at higher loads as a maximum in a_z is reached. This result is visible in the stress-strain curves that are offset but parallel to the resistance strain gauge values.

6.4 Recommendations

The effects of rigid body motion can be broken down into two categories: (1) RBM causing error in the strain measurements; and (2) RBM totally decorrelating the speckle patterns, usually leading to termination of the data run.

(1) As discussed in section 6.2, this error can be eliminated by decreasing the ratio of Lo/Ls, or limiting the term a_z at the source. The ratio Lo/Ls should be decreased by another order of magnitude to achieve acceptable results through reasonable alignment efforts. Since decreasing Lo also decreases the sensitivity of the system, the preferred choice is to increase Ls by either lengthening the optical paths or by using a lens system to position the beam waist.

For the case of a test situation where translations of the test components are extreme and unavoidable, the z translation term could be measured for

each pair of speckle patterns recorded and calculated out of the speckle shift equation.

(2) The other effect of rigid body motion is decorrelation of the reference and shifted speckle patterns. This is caused primarily by a prohibitively large component of shift in the vertical direction (A_Y), discussed as point number 6 in section 6.2. As A_Y increases, the amount of common information between the reference and shifted speckle patterns as recorded by the photodiode array becomes less and less. A clear correlation peak then becomes difficult to discern from the secondary peaks caused by the mean spatial frequency of the power density distribution.

If A_Y is a slowly varying function with respect to load, then decorrelation can be avoided by incrementing the load in small steps, and using the "relative shift" technique to compute strain. The sensitivity to A_Y can also be decreased by placing a cylindrical lens between the specimen and the linear photodiode array.

The high temperature problems of the system have to be dealt with in a different manner. Although small terms in A_Y can be eliminated with a cylindrical lens, wavering of the patterns in the X direction would have to be effectively steady-state during the retrieval of each speckle pattern pair, or else eliminated altogether. Since the speckles waver too quickly to treat as steady-state, the alternative is to suppress the cause. This should be done with baffles in the vicinity of the heated specimen, which would block convective air flow and decrease transverse thermal gradients between the specimen and the sensor.

Another improvement of the system would be to decrease the correlation time necessary to calculate the strain. The minimum time between strain points is presently about 32 sec, most of which is spent performing the correlations between the reference and shifted speckle patterns. Although this time is minimal compared to post-processing techniques, it limits the real time applications in terms of frequency response requirements. Integrating a narrower cross section of the diode array and correlating over a smaller range of shift, as well as developing a more efficient correlation algorithm, would decrease the processing time; a hardware correlator with the proper resolution would speed the calculations yet further.

Further efforts in developing this electronic speckle shift strain measurement system will include capabilities for measuring different strain axes without changing the orientation of the specimen.

APPENDIX A

EQUIPMENT LIST

Optical equipment:

- Argon-ion laser, Lexel model 95-4
- Beamsteerers, Oriel model 1450
- Beam splitter, Newport model 930-51
- Line filter, 514.5 nm peak, Oriel model 53020
- Filter holder, Oriel model 1265
- Mirror, Newport model 20Z20-DM.5
- Beam expander/collimator, Newport model LC-V-SET
- Acousto-optic modulator, IntraAction model AOM-40 w/controller model ME-40T
- Motorized mirror mount, Oriel model 18360 w/controller model 18009
- Translation stage, Oriel model 1620
- Rotator, Oriel model 1641
- Optical table, Newport model RS-58-8 w/mounting legs model XL4A-22
- Area camera, EG&G Reticon model MC528C128x128-1 w/controller model RS528
- Line scan camera, EG&G Reticon model LC120-U-2048/16 w/power supply/ data unit model RS600B
- Radiation pryometer, Ircon model 6-08C15-0-2-0-00-0/622 w/tripod model TM-6

Testing machinery:

- Stress fatigue testing machine, fatigue dynamics model DS 6000
- Induction heater, Lepel model T-2.5-1-KC1-BW(T)
- Hydraulic table, Air Technical Industries model SLI-44860-W

Computer system:

- Microcomputer controller, Hewlett-Packard model 9836CU
- Disc/tape drive (65.7 Mbyte), Hewlett-Packard model 7912P/R
- Data acquisition/control unit, Hewlett-Packard model 3497A
- Extender for the 3497A, Hewlett-Packard model 3498A
- Bus expander, Hewlett-Packard model 9888A
- Waveform recorder, Hewlett-Packard model 5180A
- Programmable function generator, Hewlett-Packard model 8116A
- Thermal printer, Hewlett-Packard model 2673A
- Plotter, Hewlett-Packard model 7475A

APPENDIX B

CUSTOM ELECTRONICS

This is a brief description of the electronics designed and built in-house. This custom electronic control system consists of three parts. Each part is implemented on a single PC board. These parts are:

(1) Custom linear camera controller (CLCC)
(2) Custom area camera controller (CACC)
(3) Custom interface control (CIC)

The control system receives signals from a digital output card in the data acquisition unit (DAQ), the area and linear array cameras, and two function generators. It sends signals to the area and linear array cameras, the two function generators, the waveform recorder, and the acousto-optic modulators (fig. B-1).

Figure B-2 shows the three parts of the control system with the input and output signals on each board. A waveform recorder (WFR) is being used to store the data before processing it in the computer. The three signals that determine the timing for recording the data (video information) are: ENABLE (WFR trigger), clock, and data itself. Those signals were synchronized at the WFR input in order to sample the video in the middle of a pulse and avoid transient data. Also, to avoid corrupted data, the controls will ignore the first video frame after changing state and be ready for recording after that. Simplified timing diagrams for the area and linear camera controls are shown in figures B-3 and B-4, respectively. The area camera uses its own internal start pulse while the linear camera uses an external start pulse supplied by the linear camera controller board.

Custom Area Camera Control Circuitry

This circuit is responsible for providing the modulation signals for the linear and area (expanded) laser beams, using programmable function generators.

The area camera uses its internal start signal. Therefore, the scanning time (Tas) is fixed according to the clock frequency. The equation for Tas is as follows:

$$Tas = \frac{(128 \text{ by } 128 + 25)}{f}$$

where 128 by 128 is the number of photodiodes in the area array, 25 is the number of pulses between the end of the scan and the next start pulse, and f is the camera clock frequency (set to 1.02 MHz) (ref. 6).

Also, the area camera controller sends, at a specific time, the ENABLE signal from the area camera to the WFR which stores the video output in digital form. For more details, see the area camera control timing diagram (fig. C).

Custom Linear Camera Control

The CLCC circuitry provides the control signals for the left and right acousto-optic modulators. These controls are ORed with the linear controls (A_L, A_R) of the area camera.

The linear camera uses an external start signal. This signal is provided by the custom circuitry at the end of the function generator's exposure pulse. Thus, the scan time T_{LS} is externally controllable by the exposure pulse width. The minimum value of T_{LS} is given by

$$Tsmin = \frac{(2048 + 4)}{f}$$

where 2048 is the number of photodiodes in the array, 4 is the number of clock pulses between the start pulse and the positive edge of the ENABLE signal, and f is the clock frequency (ref. 7). The maximum scan time (T_{LMAX}) is 40 ms, after which dark current in the photodiodes becomes significant.

This circuitry also sends the ENABLE signal of the linear camera to the WFR, which stores the video information as digital data. For more details, see the Linear Camera Control Timing Diagram (fig. D).

The Interface Circuit

This circuit provides the following:

(1) A start signal that does not trigger the function generator, yet keeps the linear camera running. This was done to avoid introducing a start signal each time Pr.LN goes LOW.

(2) Conversion from differential form to single ended form, for the following signals:

(a) ENABLE of the area camera (EN_A)
(b) ENABLE of the linear camera (EN_{LN})
(c) Video signal
(d) Clocks for both the area and linear cameras (CL_A, and CL_{LN}).

(3) OR function, so that the waveform recorder used either the area or linear clock at one time.

(4) Delay in the clock path, to achieve the sampling in the middle of the video pulse. This synchronization is important to avoid transients at either end of the video pulse.

The responsibilities of this circuit include sending the clock signals of both the area and linear cameras, and the video information.

Most of the circuitry uses CMOS IC's. However, some TTL components were used for fast switching, especially in the clock signal paths.

REFERENCES

1. Yamaguchi, I.: A Laser-Speckle Strain Gauge. J. Phys. E. Sci. Instrum., vol. 14, no. 11, Nov. 1981, pp. 1270-1273.

2. Stetson, K.A.: Demonstration Test of Burner Liner Strain Measuring System. (R84-926376-15, United Technologies Research Center; NASA Contract NAS3-23690) NASA CR-174743, 1984.

3. Sharpe, W.N., Jr.: In-Plane Interferometric Strain/displacement Measurement at High Temperatures. Measurements in Hostile Environments, British Society for Strain Measurement, Newcastle Upon Tyne, England, 1981.

4. Yamaguchi, I.: Speckle Displacement and Decorrelation in the Diffraction and Image Fields for Small Object Deformation. Optica Acta, vol. 28, no. 10, Oct. 1981, pp. 1359-1376.

5. Goodman, J.W.: Laser Speckle and Related Phenomena, J. C. Dainty, ed., Springer-Verlag, 1975, pp. 39-40.

6. Operation and Maintenance Manual, MC520/RS520 Camera/Controller System. EG∂G Reticon, Sunnyvale, CA.

7. Operation and Maintenance Manual, LC120 Line Scan Camera. EG∂G Reticon, Sunnyvale, CA.

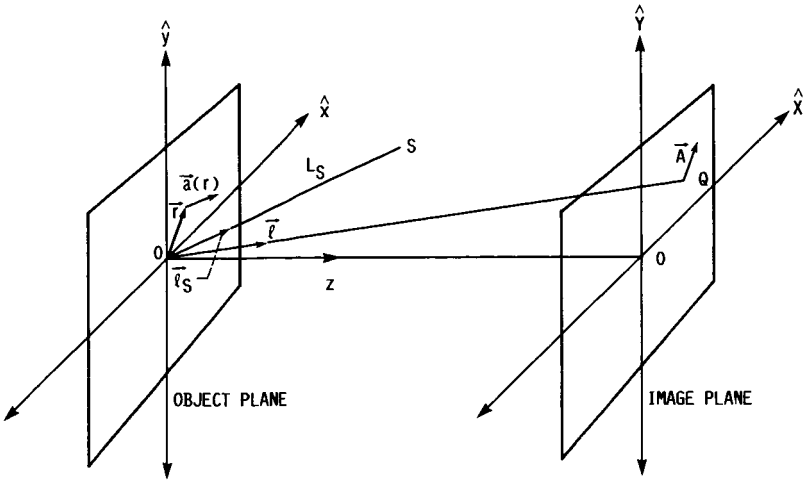

FIGURE 1. - GENERAL COORDINATE SYSTEM.

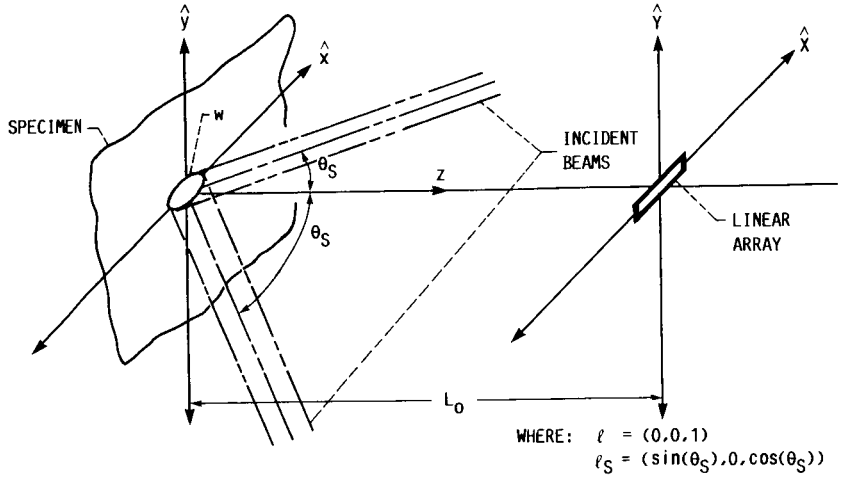

FIGURE 2. - SIMPLIFIED BEAM AND SENSOR ARRANGEMENT.

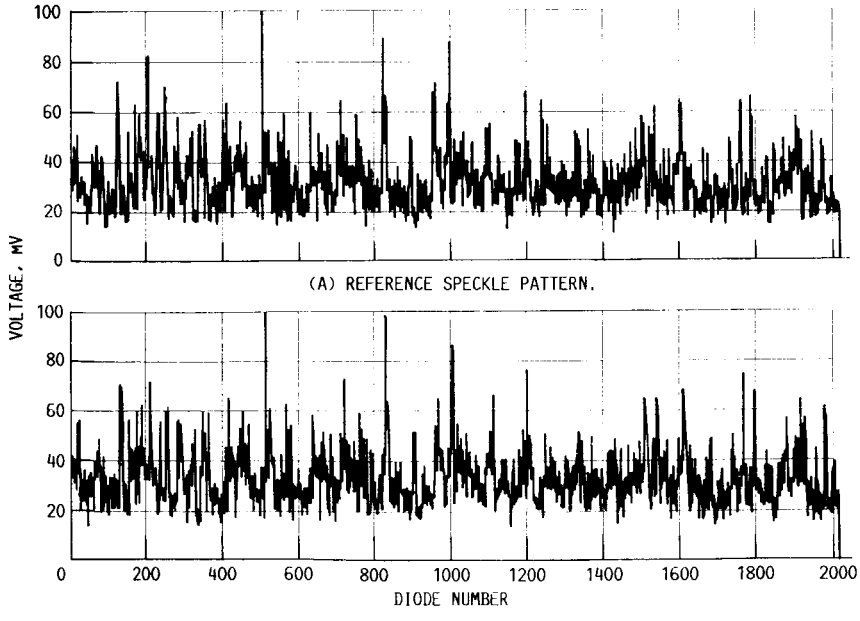

(A) REFERENCE SPECKLE PATTERN.

(B) SHIFTED SPECKLE PATTERN.

FIGURE 3. - TYPICAL PAIR OF REFERENCE AND SHIFTED SPECKLE PATTERNS.

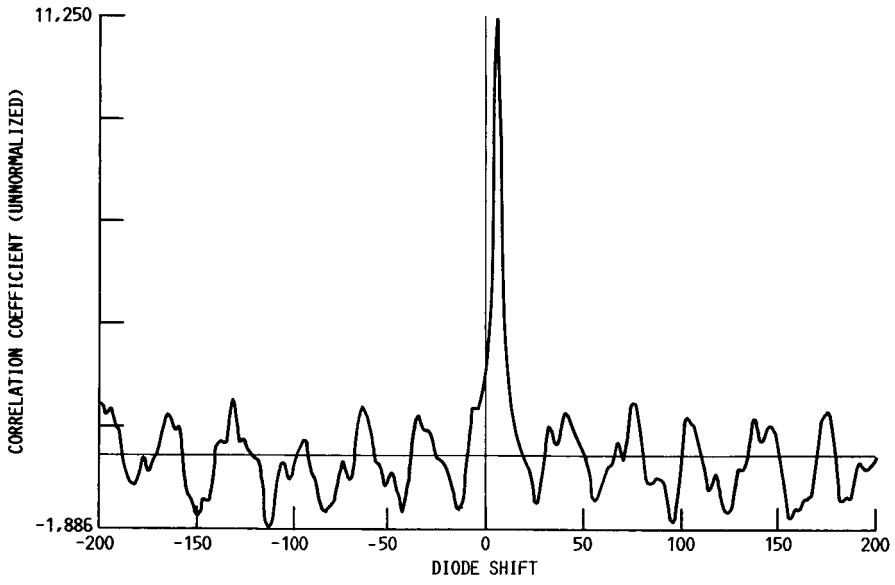

FIGURE 4. - CORRELATION OF SPECKLE PATTERNS IN FIGURE 3.

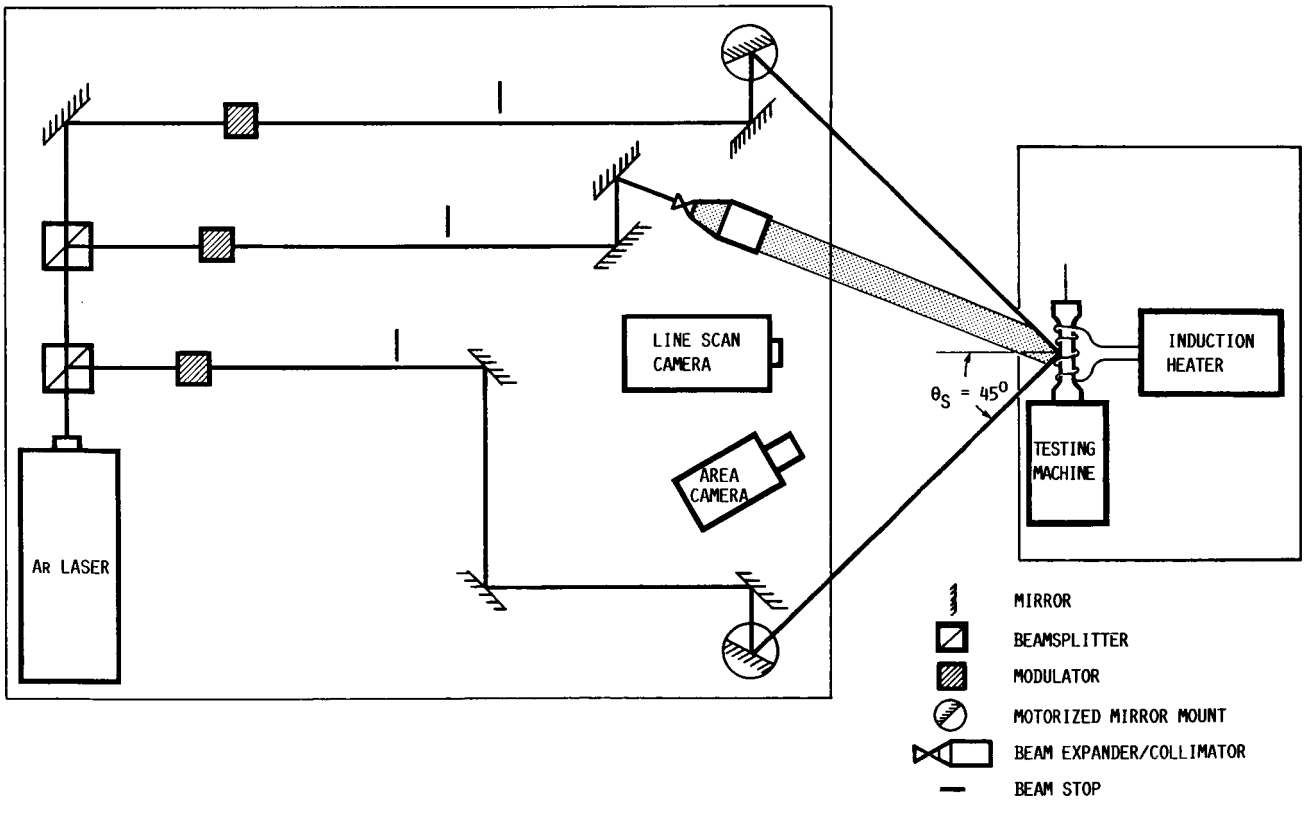

FIGURE 5. - OPTICAL SETUP AND TEST EQUIPMENT.

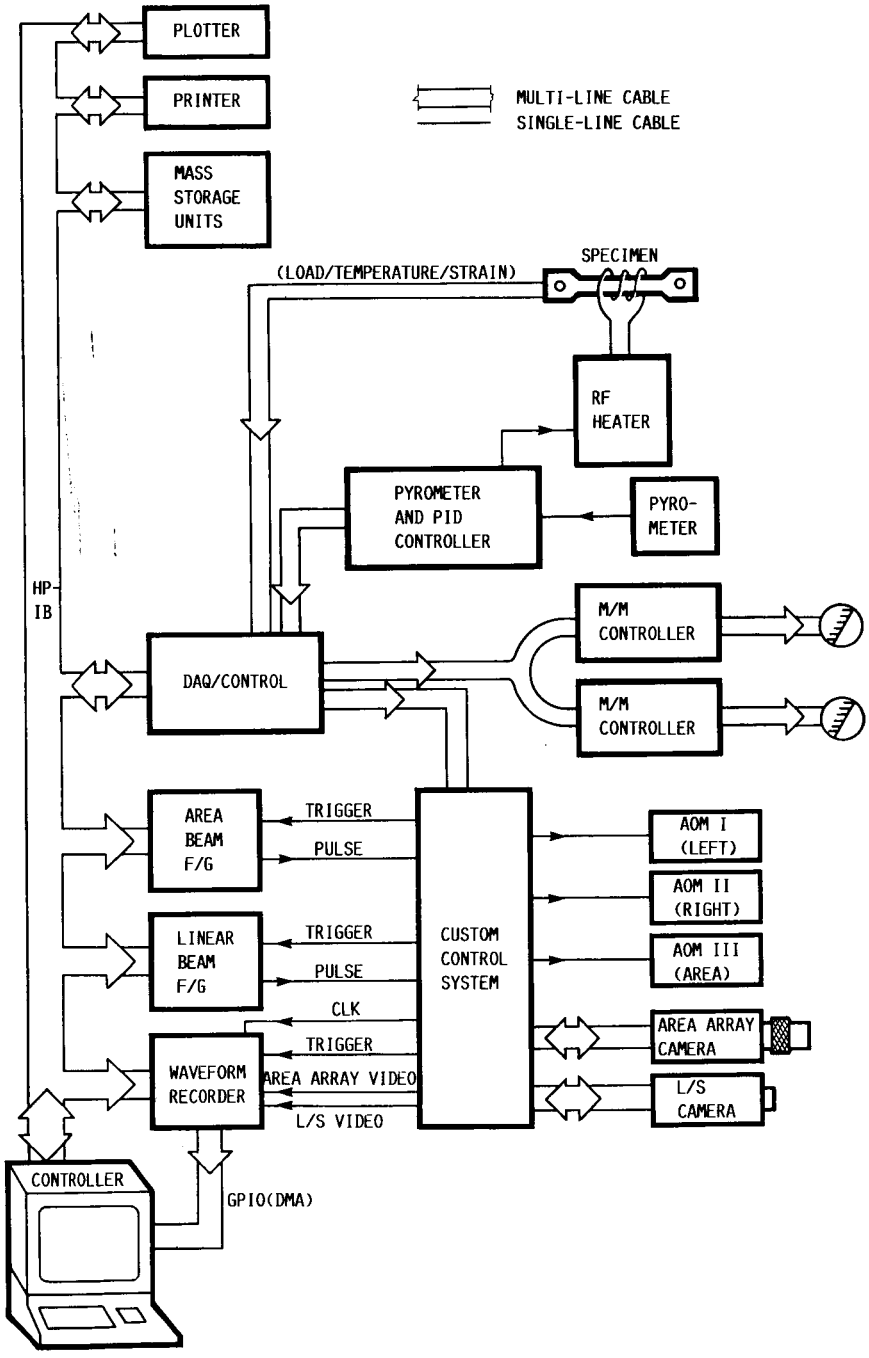

FIGURE 6. - BLOCK DIAGRAM OF THE CONTROL/DATA ACQUISITION SYSTEM.

ORIGINAL PAGE IS
OF POOR QUALITY

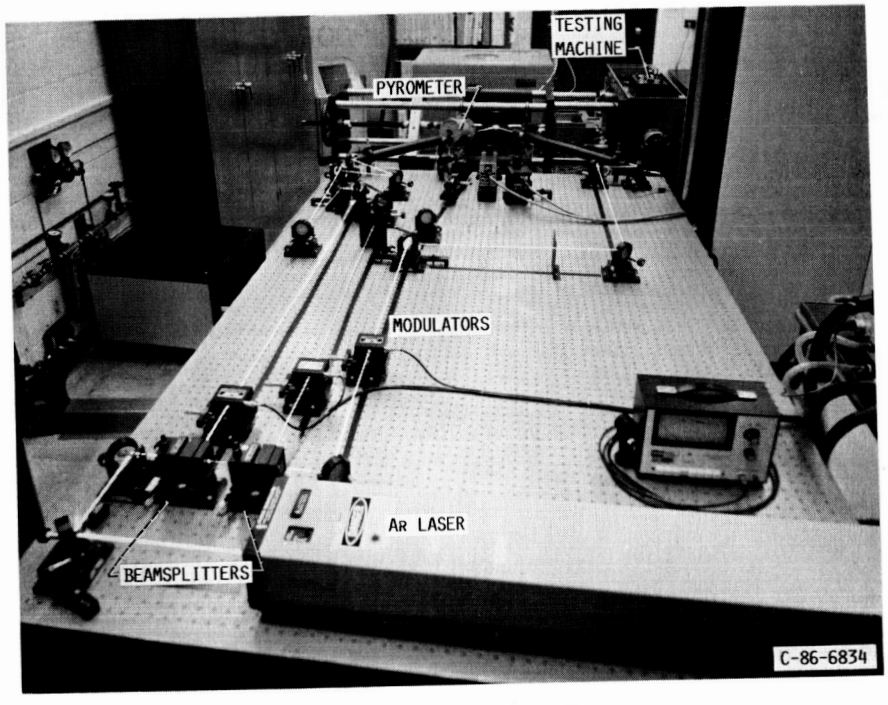

FIGURE 7. - OPTICAL SYSTEM

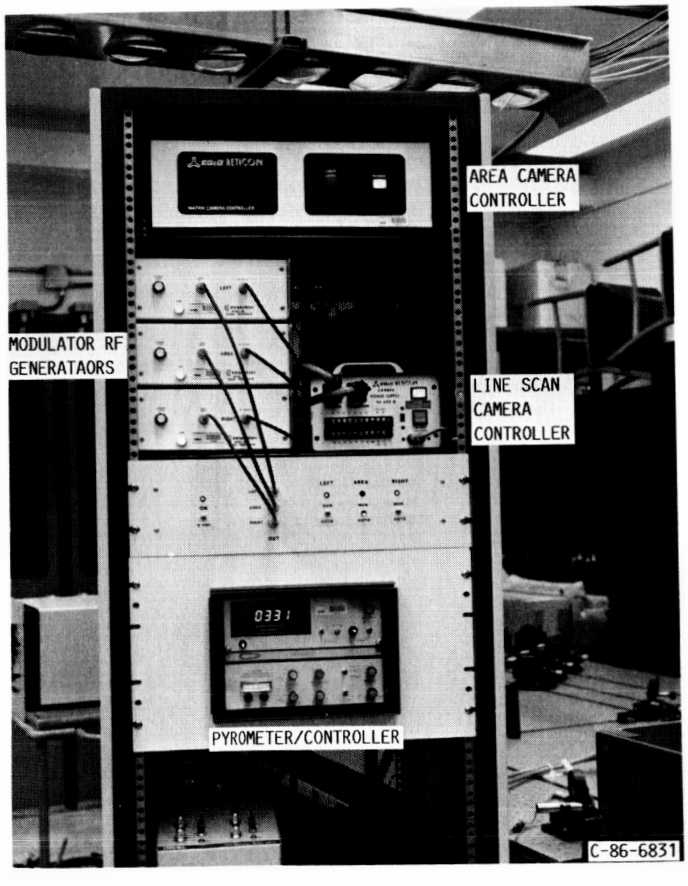

FIGURE 8. - ANALOG CONTROL RACK.

ORIGINAL PAGE IS
OF POOR QUALITY

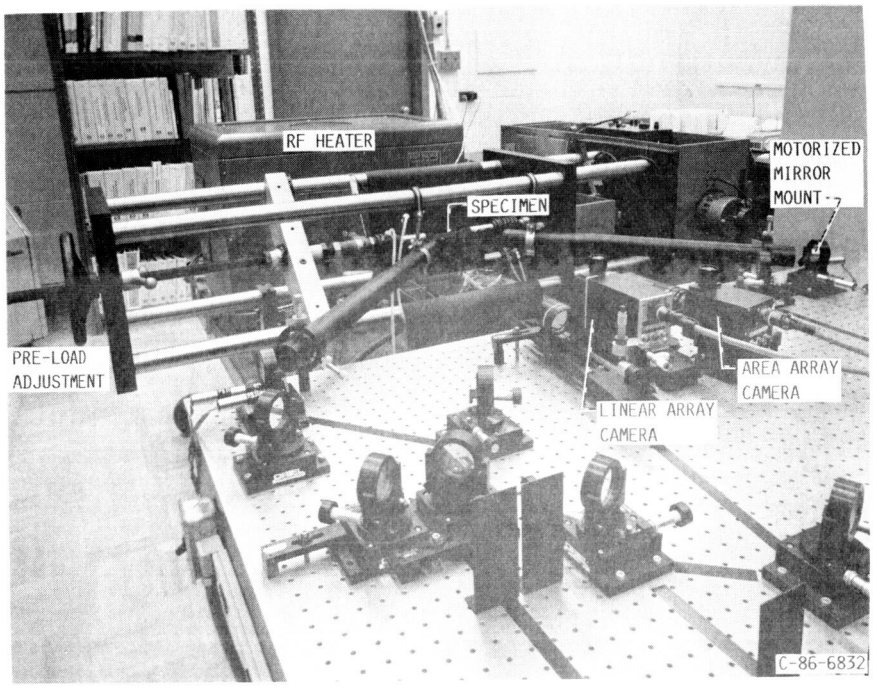

FIGURE 9. - TEST SYSTEM.

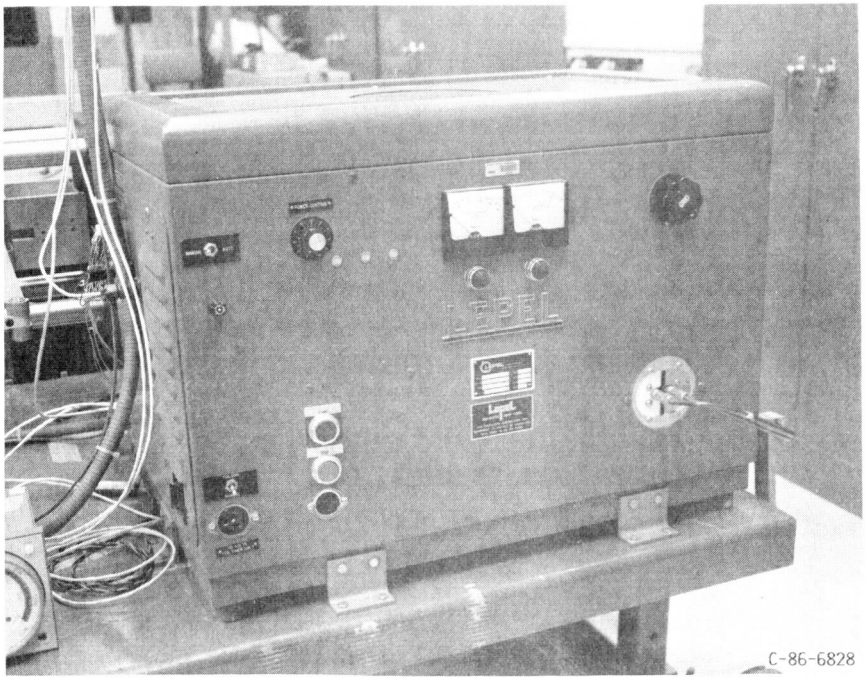

FIGURE 10. - RF HEATER.

ORIGINAL PAGE IS
OF POOR QUALITY

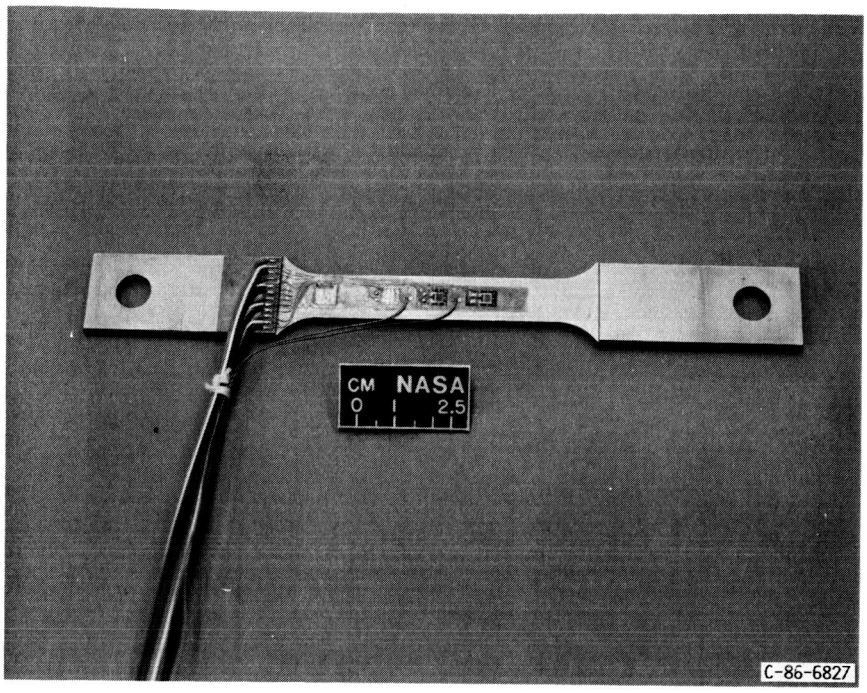

FIGURE 11. - SPECIMEN NUMBER 1.

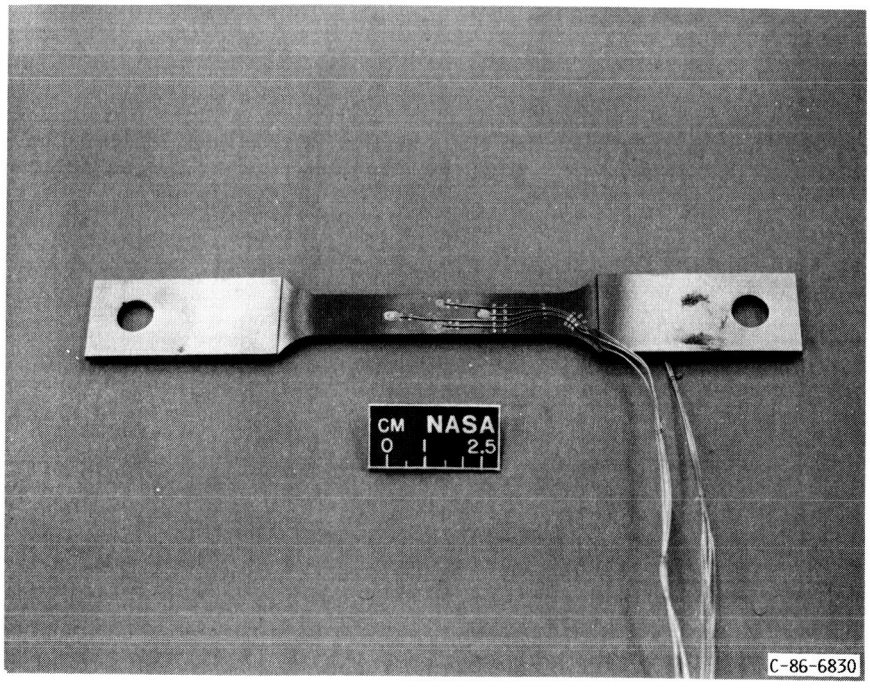

FIGURE 12. - SPECIMEN NUMBER 2.

ORIGINAL PAGE IS
OF POOR QUALITY

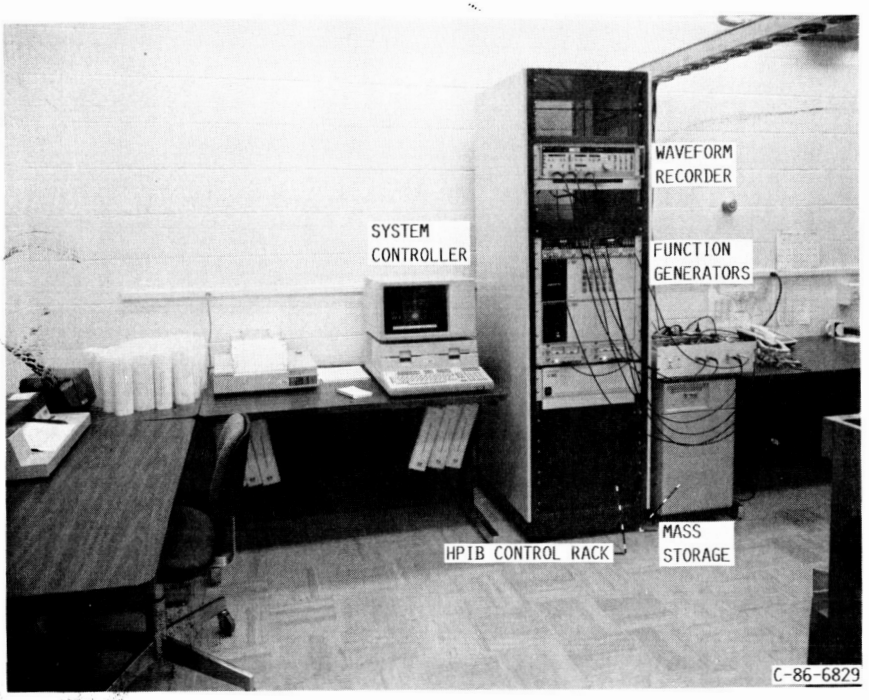

FIGURE 13. - CONTROL STATION (COMPUTER EQUIPMENT).

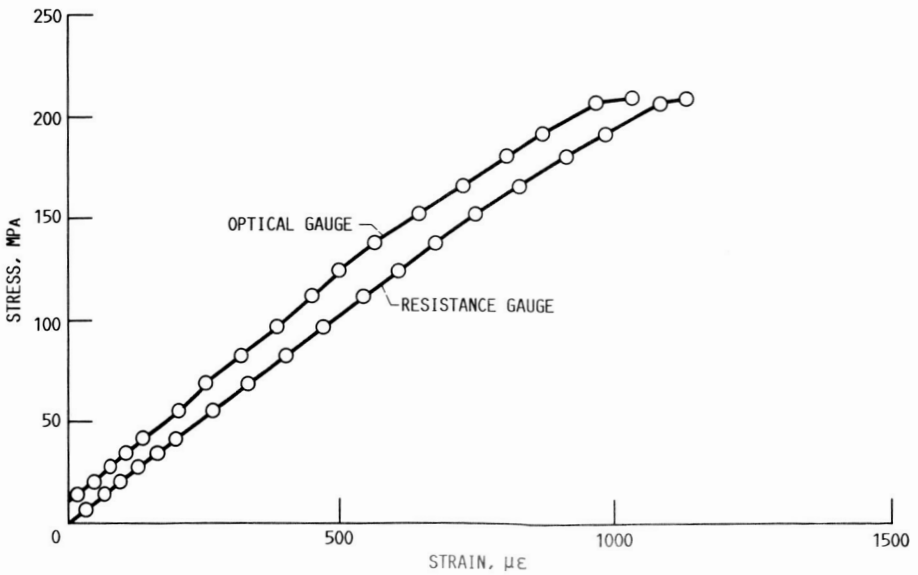

FIGURE 14. - COMPARISON OF OPTICAL GAUGE WITH RESISTANCE GAUGE AT ROOM TEMPERATURE.

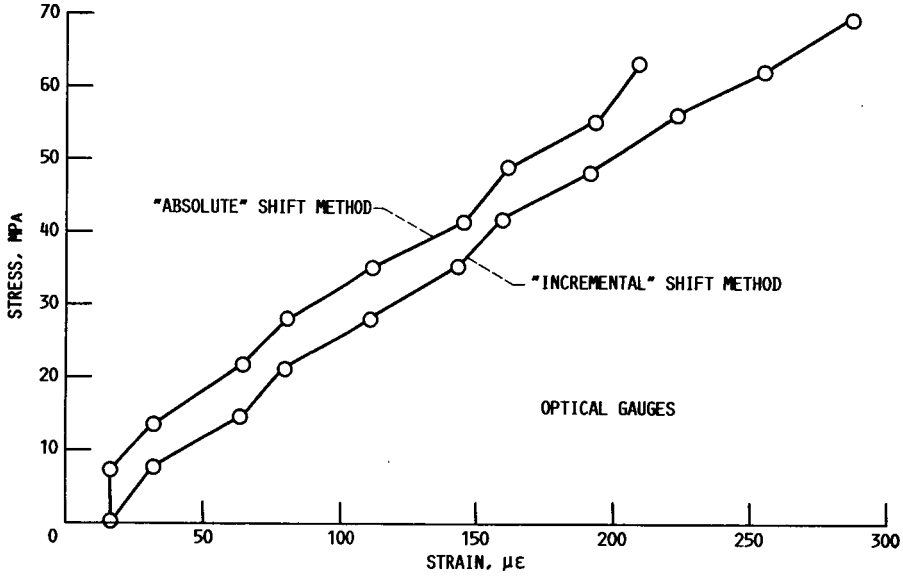

FIGURE 15. - COMPARISON OF THE "ABSOLUTE" SHIFT METHOD WITH THE "INCREMENTAL" SHIFT METHOD, AT ROOM TEMPERATURE.

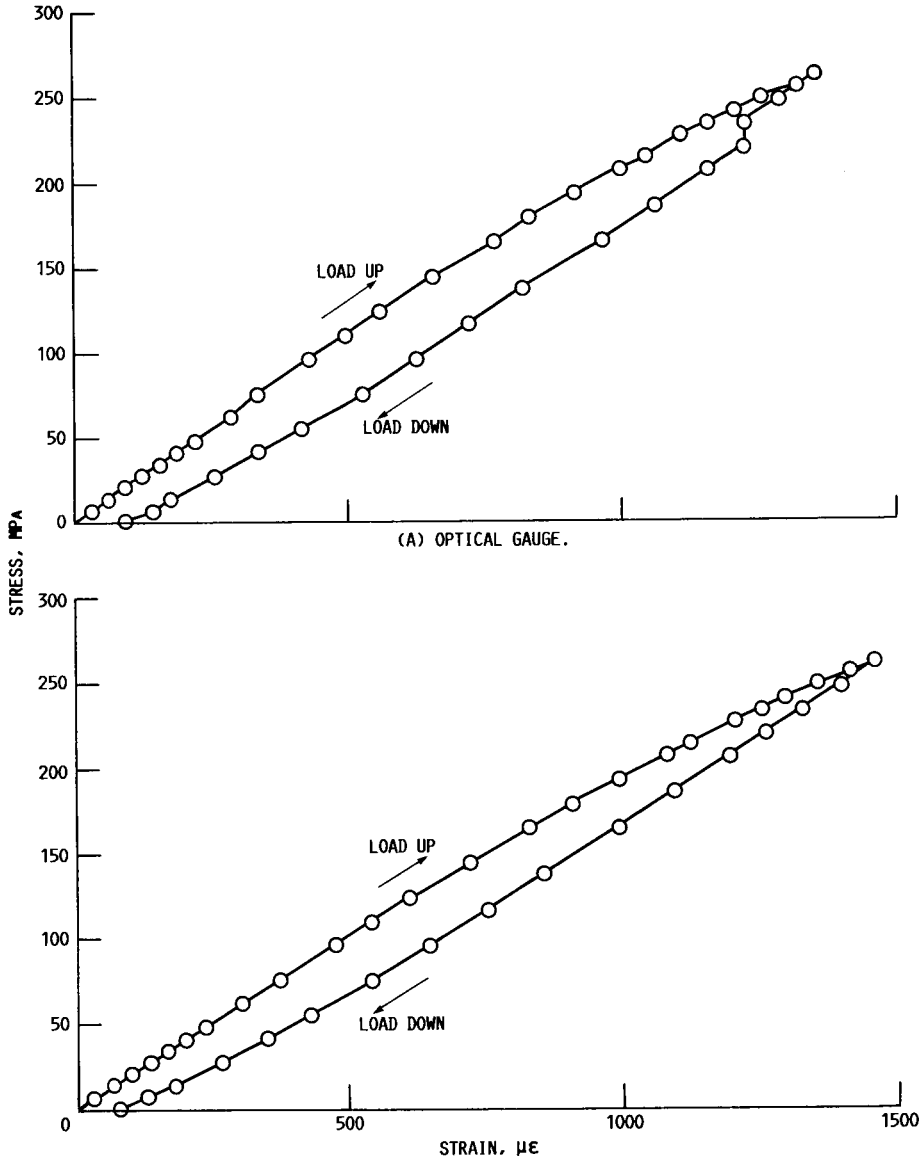

FIGURE 16. - HYSTERESES OF THE OPTICAL AND RESISTANCE GAUGES.

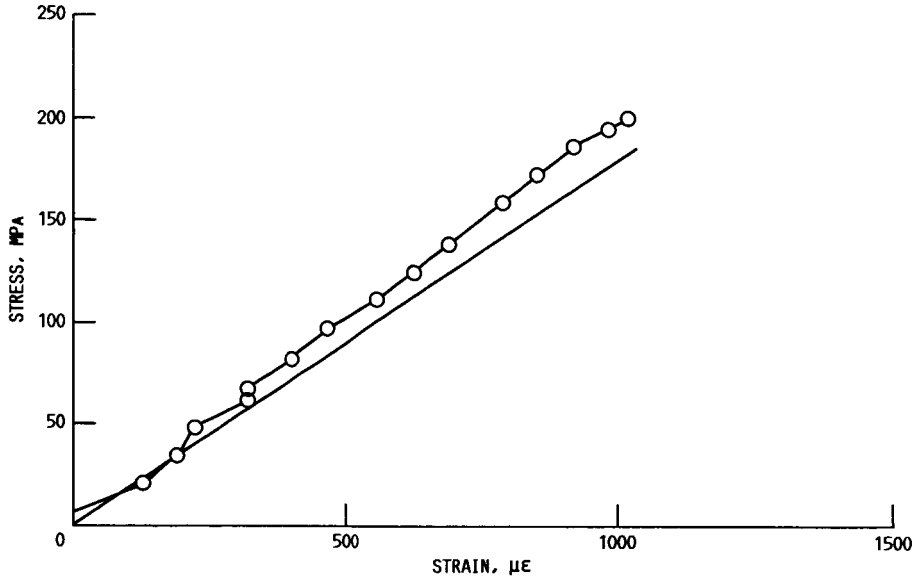

FIGURE 17. - OPTICAL GAUGE DATA AT 450 ^{o}C.

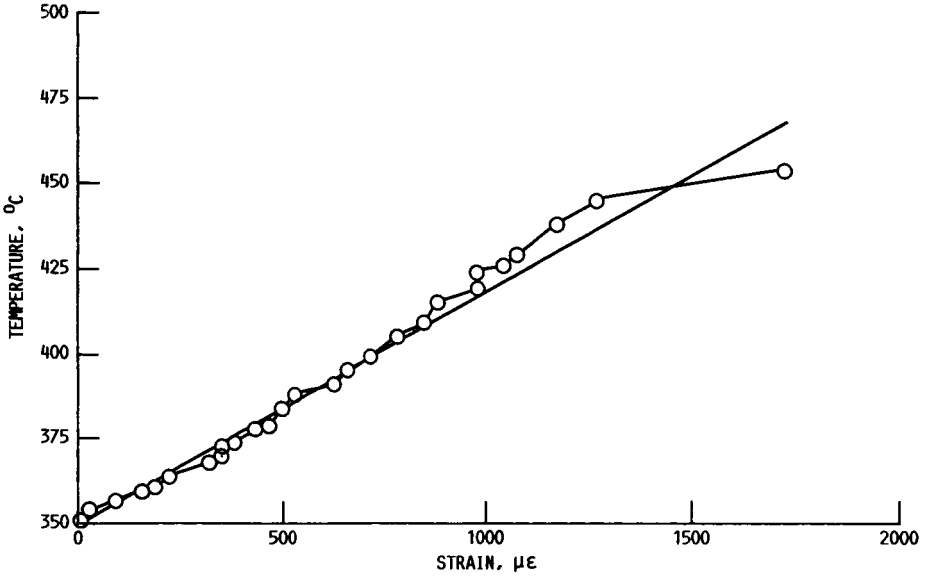

FIGURE 18. - OPTICAL MEASUREMENTS OF THERMAL STRAIN. THE STRAIGHT LINE INDICATES THE HANDBOOK COEFFICIENT OF THERMAL EXPANSION.

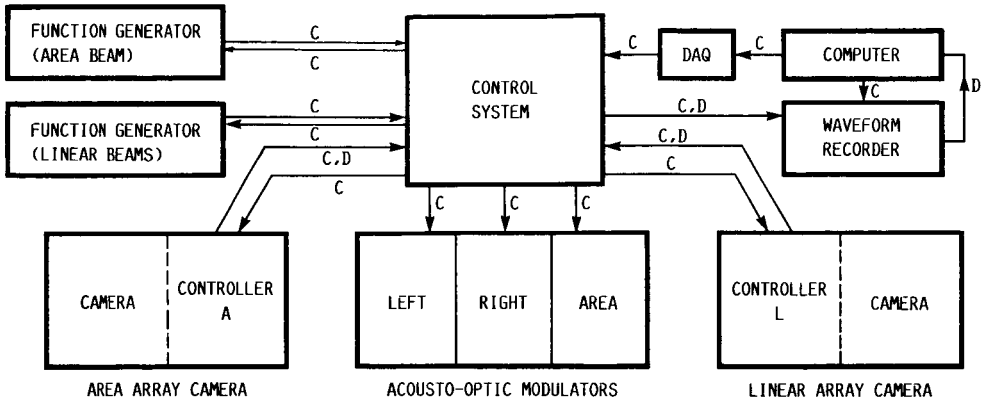

NOTES:
1 - ARROWS SHOW FLOW OF INFORMATION
2 - D: DATA
C: CONTROL
3 - CONTROLLERS L AND A ARE DIFFERENT FROM THE CONTROLLERS IN THE CONTROL BOX

FIGURE B-1. - ELECTRICAL SYSTEM BLOCK DIAGRAM.

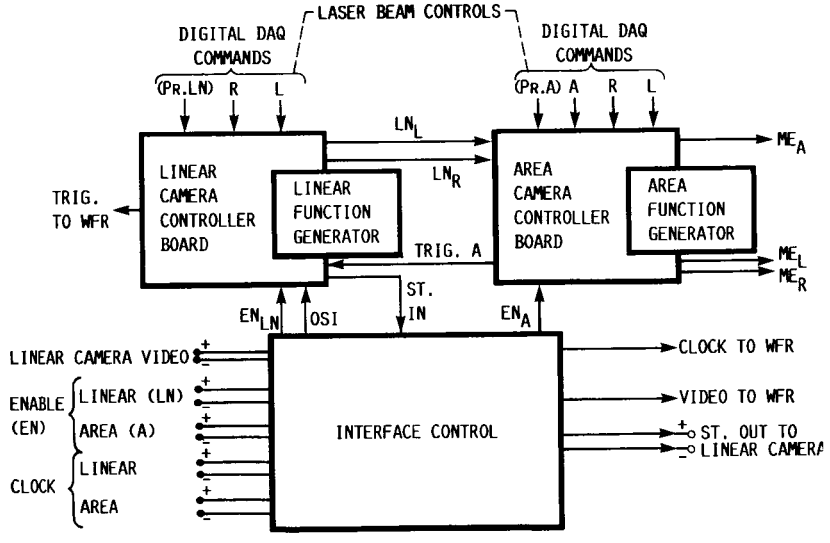

LEGEND:
ME - BEAM MODULATOR, LN - LINEAR
A - AREA, L - LEFT, R - RIGHT
LN_L - LEFT BEAM CONTROL OF LN CAMERA
LN_R - RIGHT BEAM CONTROL OF LN CAMERA
PR - PRESET, WFR - WAVEFORM RECORDER
ST - START SIGNAL

FIGURE B-2. - CONTROL SYSTEM BLOCK DIAGRAM (CONTROL BOX).

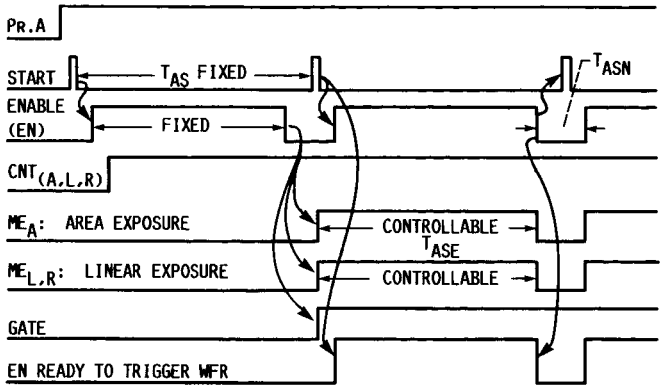

NOTES:

1 - $T_{AS} = T_{ASE} + T_{ASN}$

2 - T_{ASE} IS CONTROLLABLE AND T_{ASN} IS FIXED

3 - $EN = \frac{128x128}{f}$

4 - f IS FREQUENCY OF CAMERA CLOCK

FIGURE B-3. - AREA CAMERA CONTROL TIMING DIAGRAM.

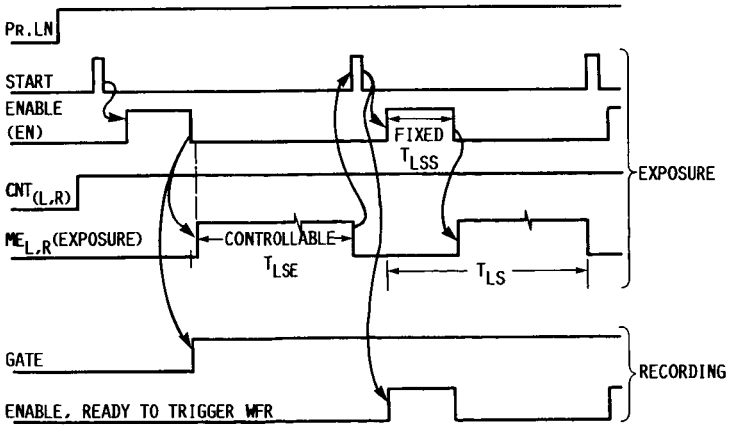

NOTES:

1 - $T_{LS} = T_{LSE} + T_{LSS}$

2 - FOR COMPLETE CYCLE PR.LN SHOULD BE "HIGH"

3 - EN = 2048/f

4 - f IS CLOCK FREQUENCY OF THE CAMERA

FIGURE B-4. - LINEAR CAMERA CONTROL TIMING DIAGRAM.

1. Report No.	2. Government Accession No.	3. Recipient's Catalog No.
NASA CR-179619		

4. Title and Subtitle	5. Report Date
Optical Strain Measurement System Development - Phase I	May 1987
	6. Performing Organization Code

7. Author(s)	8. Performing Organization Report No.
Christian T. Lant and Walid Qaqish	None (E-3550)
	10. Work Unit No. 506-42-11

9. Performing Organization Name and Address	11. Contract or Grant No.
Sverdrup Technology, Inc. Lewis Research Center Cleveland, Ohio 44135	NAS3-24105
	13. Type of Report and Period Covered Contractor Report Final

12. Sponsoring Agency Name and Address	14. Sponsoring Agency Code
National Aeronautics and Space Administration Lewis Research Center Cleveland, Ohio 44135	

15. Supplementary Notes

Project Manager, John P. Barranger, Instrumentation and Control Technology Office, NASA Lewis Research Center.

16. Abstract

A laser speckle, differential strain measurement system has been built and tested for future applications in hostile environments. One dimensional electronic correlation of speckle pattern movement allows a quasi-real time measure of strain. The system has been used successfully to measure uniaxial strain reaching into plastic deformation of a test specimen, at temperatures ranging to 450 °C. A resolution of 16 microstrain is given by the photodiode array sensor pitch and the specimen to sensor separation. The strain measurement error is ±18 microstrain ±0.3 percent of the strain reading. The upper temperature limit of the gauge is determined by air density perturbations causing decorrelation of the reference and shifted speckle patterns, and may be improved by limiting convective flow in the immediate vicinity of the test specimen.

17. Key Words (Suggested by Author(s))	18. Distribution Statement
Laser speckle; High temperature strain measurement; Correlation; Diffraction; Refraction	Unclassified - unlimited STAR Category 35

19. Security Classif. (of this report)	20. Security Classif. (of this page)	21. No. of pages	22. Price*
Unclassified	Unclassified	38	A03

*For sale by the National Technical Information Service, Springfield, Virginia 22161